DOI: 10.13009/EUCASS2017-468

Quasi-steady and Forced Transient Burning of a Vortex Flow Hybrid Motor

Christian Paravan, Stefania Carlotti, Filippo Maggi, and Luciano Galfetti
Politecnico di Milano, Aerospace Science and Technology Dept.,
Space Propulsion Laboratory (SPLab),
34, via LaMasa, 20156, Milan, Italy

Abstract

The current development status of a vortex flow pancake (VFP) hybrid rocket engine is presented. The characterization of the VFP configuration is focused on internal flow-field investigation and combustion behavior analysis. The internal flow-field is characterized by highspeed visualizations and numerical analyses showing the effects of oxidizer mass flow rate ($\dot{m}_{ox}$) and combustion chamber height on the vortex structure. Quasi-steady and forced transient combustion runs were performed to investigate the motor behavior. The forced transient test showed a stable behavior of the VFP, without combustion chamber pressure undershoot/overshoot because of the throttle up after $\dot{m}_{ox}$ interruption.

1. Introduction

Hybrid rocket engines (HREs) are thermochemical propulsion systems featuring oxidizer and fuel in different states of matter. This configuration offers attractive features as high theoretical specific impulse (I_s) values, high operating flexibility (i.e., multiple ignitions, thrust throttling), and high safety levels (in turn yielding recurring cost reduction thanks to the easy manufacturing and transportation of the motor) [1]. Nevertheless, HRE development has been so far hampered by their intrinsically low regression rate (r_f) and poor combustion efficiency. The low r_f is considered a drawback, when focusing on applications requiring high thrust levels (i.e., large launch systems). Nevertheless, there are several emerging mission profiles and requirements in in-space propulsion, where the thrust level is not a driver. In these scenarios, the main figures of merit is the I_s and operating flexibility, and reliability and safety are key factors. Thus, HRE implementations granting improved combustion efficiencies may represent a breakthrough for these applications.

This paper discusses an innovative motor configuration originally proposed by the Surrey Space Center [2]: the vortex flow pancake (VFP). In this non-conventional motor geometry, a tangential oxidizer injector is sandwiched between two fuel disks. One of the disks features a central port connecting the combustion chamber to the gasdynamic nozzle. With this implementation large surface areas can be achieved with a simple design and with a combustion chamber length-to-diameter ratio (L/D) < 1. The tangential injection of the oxidizer induces a vortex flow-field in the gap between two solid fuel disks. Hence, the mixing between fuel and oxidizer is enhanced, leading to possible combustion efficiency enhancements. The VFP considered in the study was designed, implemented and tested at the Space Propulsion Laboratory (SPLab) of Politecnico di Milano. The system, named SPLab vortex flow pancake (SVFP), was realized based on the model presented in Ref. 2. The system internal flow-field was investigated numerically to evaluate the oxidizer-fuel mixing under different oxidizer injection configurations and operating conditions, considering cold-flow conditions. The motor combustion behavior was investigated by combustion runs performed under quasi-steady and forced operating conditions. This work represents an initial assessment of the SVFP performance [3].

1.1 Literature Survey

The combustion process of solid fuels with an atomized/gaseous oxidizer flowing along the condensed phase surface was the object of intense studies during the 1960s, and has recently been extended [1][4-8]. The turbulent boundary layer combustion of polymeric fuels in standard flow configurations was detailed investigated by Marxman and co-workers [4-6]: the oxidizer flows over the solid fuel grain generating a boundary layer. After ignition, a diffusion flame is set in this region. The heat transfer from the flame to the condensed phase is mainly due to convection and promotes the fuel gasification [4-6]. Thus, the regression rate of the solid fuel depends mainly on the overall oxidizer mass flux, sum of the oxidizer and of the fuel components along the grain port [$G(x) = G_{ox} + G_f(x)$], $r_f \sim G(x)^{0.8}$. The heat transfer process is hindered by the mass blowing effect from the condensed phase. Thus, the effective heat transfer coefficient is reduced [4-6]. This, in addition to the diffusion phenomena involved in the combustion process, yields the intrinsic solid fuel regression rate limitation characterizing the HRE combustion process. The turbulent boundary layer

DOI: 10.13009/EUCASS2017-468

combustion model based on the solid fuel gasification has been recently extended for particular fuel formulations [7,8]. Solid fuels whose melted phase exhibits low viscosity and surface tension show inherently high r_f thanks to the entrainment of liquid phase droplets. While showing promising features toward the design of high-thrust systems, the fuels producing entrainment (i.e., cryogenic hybrids, solid paraffin waxes) exhibit poor mechanical properties (or complex design) hindering their possible applications in affordable operating systems. The r_f enhancement (crucial for the application of HRE to high-thrust missions), is currently pursued by different approaches as solid fuel loading with energetic additives [9-10], and exotic oxidizer injection techniques [11-15].

Non-conventional injection techniques and exotic grain configurations may yield augmented performance in terms of solid fuel r_f and combustion efficiency by increasing flow turbulence in the flame-surface heat transfer process. The two approaches may also be used in conjunction [1]. In exotic injection techniques applied to conventional motor configurations (cylindrical grains with L/D > 1), the oxidizer inlet configuration promotes a vortex flow whose effects are a heat transfer enhancement thanks to the augmented velocity components (parallel and tangential to the fuel grain longitudinal axis), improved propellant mixture mixing and residence time. Yuasa et al. [11] investigated swirling head-end injection effects on the r_f of PMMA-O_2. Injector implementations with different geometrical swirl number were tested to determine the independent effects of injection condition and G_{ox} on the fuel r_f. Thanks to the swirl injection with geometrical swirl number (S_g) up to 19.4, the measured solid grain r_f resulted up to 2.7 times higher than achieved by standard-flow inlet under similar operating conditions. Different grain lengths (150 mm and 500 mm) were tested in [11]. The main limitation of this approach is the swirl intensity decay due to the viscous dumping along the solid fuel grain length, and the tangential component loss induced by the surface mass blowing [15]. Different solutions were proposed to limit this effect: helical fuel grains [13], the use of tapered grain configurations [14], the implementation of multiple injectors along the fuel grain [15]. Exotic vortex flow HRE configurations were proposed by Gibbon et al. [2], Knuth et al. [12], and Rice et al. [16]. A vortex flow HRE with oxidizer tangential injection was tested at the Surrey Space Center and is described in [2]. This configuration yields a very compact HRE, since high fuel gasification surface area can be achieved by increasing the combustion chamber diameter, and not the engine length. The experiments discussed in [2] show the influence of oxidizer mass flow rate and stream velocity on the burning behavior of the system. Though no detailed $r_f(G_{ox})$ was reported in the work, several experimental results showing the neutral r_f burning and the high combustion efficiency of the system were discussed. Researchers from the Orbital Technology Corporation (ORBITEC) tested non-conventional HRE with swirled aft-end injection. In the implementation discussed in [12], the oxidizer (gaseous oxygen, GOX) is injected by tangential inlets placed just above the nozzle. The GOX vortex stream moves from the aft-end to the (closed) fore-end of the central port of the fuel grain. From here the vortex moves downward from the HRE head-end to the exhaust. This double vortex flow-field promotes an intense mixing in the combustion chamber and an increased r_f. Further details on this motor configuration are reported in [1, 12]. A configuration like the one tested at the Surrey Space Center was investigated by Rice et al. [16]. In this study, the motor configuration was that of a VFP were the nozzle-side fuel grain was absent, thus realizing an end-burning configuration with aft-end injection. Under the investigated operating conditions, the oxidizer inlet velocity and the injector-regressing surface distance were found to influence the measured r_f, while no effect of the combustion chamber diameter was captured by the data reduction. Rice et al. evaluated a power-law approximation $r_f(G_{ox}) = 0.40\ G_{ox}^{0.62}$, with a pre-exponential factor that results one order of magnitude higher than that of conventional cylindrical central-perforated grains [1, 16]. Detailed numerical analyses on the internal flow-field of vortex-flow HRE are discussed by Majdalani in [17].

2. The SPLab Vortex Flow Pancake

The SVFP is shown in Figure 1 [3]. Two opposite fuel disks are faced to the injector ring and limit the combustion chamber volume. Injection is performed by four tangential (and equally spaced) inlets placed on the lateral surface of the combustion chamber. Both the fuel disks exhibit a donut-like shape, with a central port perforation. One of the two ports hosts the pyrotechnic primer charge igniting the motor grains, the second port enables the flow of the combustion products toward the nozzle. The system is completed by two flanges. One of them is connected to the water-cooled nozzle, while the other lodges the igniter. Both flanges enable the integration of sensors (e.g., thermocouples, wire-cut r_f sensors). The combustion chamber pressure (p_c) is measured by a piezo-resistive pressure transducer, while the oxidizer mass flow rate ($\dot{m}_{ox}$) is monitored by a digital flowmeter.

DOI: 10.13009/EUCASS2017-468

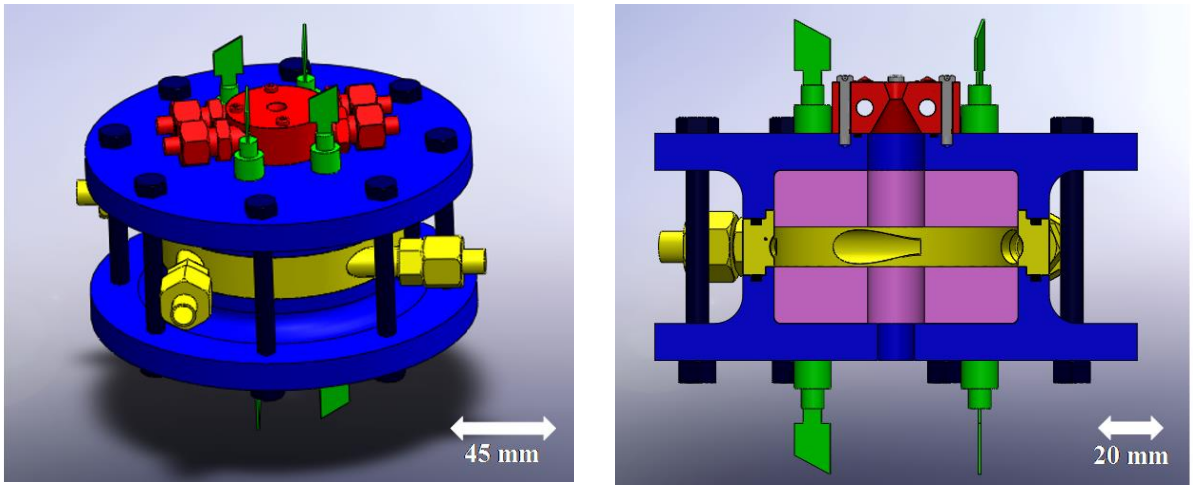

a **b**

Figure 1: Overview of the SVFP configuration (a) external and (b) cross section views: flanges and fuel grain holders (blue), injection ring (yellow), solid fuel grain (violet), water-cooled nozzle (red), and sensors (green).

2. The SVFP Internal Flow-field

The SVFP internal flow-field was investigated by numerical simulations performed in OpenFOAM®. The meshed domain is shown in the Figure 2. The grid for the computation fits to the motor sizes, with the only exception of the nozzle. The different shape of the mesh nozzle with respect to the real one is due to numerical problems encountered for the expanding flow. The numerical analyses focused on two main aspects: the vortex structure evolution during the burning due to the combustion chamber height (H_c) changes, and on the evaluation of the oxidizer/fuel mixing due to the vortex flow. Different oxidizer mass flow rates and combustion chamber heights (volumes) were investigated. The test conditions include $\dot{m}_{ox}$ from 5 to 10 g/s, and H_c of 14 mm, 34 mm and 54 mm (representing the initial burning configuration, the condition achieved after fuel web thickness half consumption, and the spacing of the SVFP regressing surfaces at the engine burnout). In the simulations, p_c = 1.0 MPa, while the oxidizer flow temperature is 300 K. Finally, the mass blowing of C_4H_6 is considered in the analysis (assuming a fuel r_f of 1.0 mm/s).

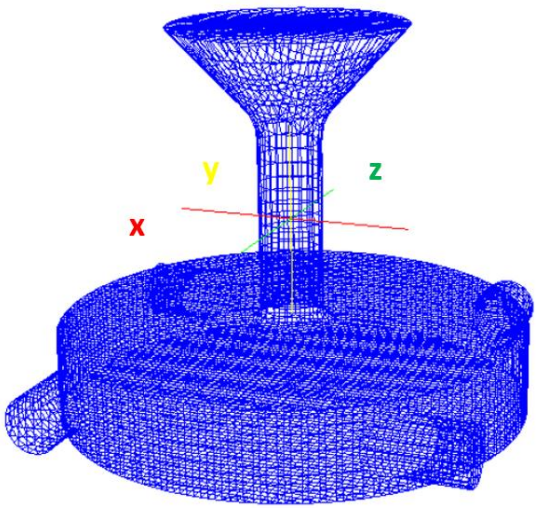

Figure 2: Meshed SVFP configuration.

DOI: 10.13009/EUCASS2017-468

The Figure 3 shows representative results for the velocity field achieved for the most representative cases. Considering the effect of the mass flow rate on the velocity distribution for H_c = 14 mm, and at burnout. The results reported in Figure 3 show the more intense velocities achieved with the higher $\dot{m}_{ox}$. Under the investigated conditions, these higher velocities imply higher friction and, therefore, a more effective heat transfer as well as a better mixing of the propellant mixture. Focusing on the combustion chamber height effects, the cold flow simulations show an effect of the latter parameter on the vortex flow-field. The achieved results suggest that during the burning, the vortex structure is altered by the increasing combustion chamber volume. Contrasting the images reported in Figure 3, the velocity of the vortex shows an outer, slower region whose insurgence is related to the augmented H_c. Results achieved under similar operating conditions, with combustion chamber height of 34 mm show an intermediate behavior with respect to the 14 mm and the 54 mm cases.

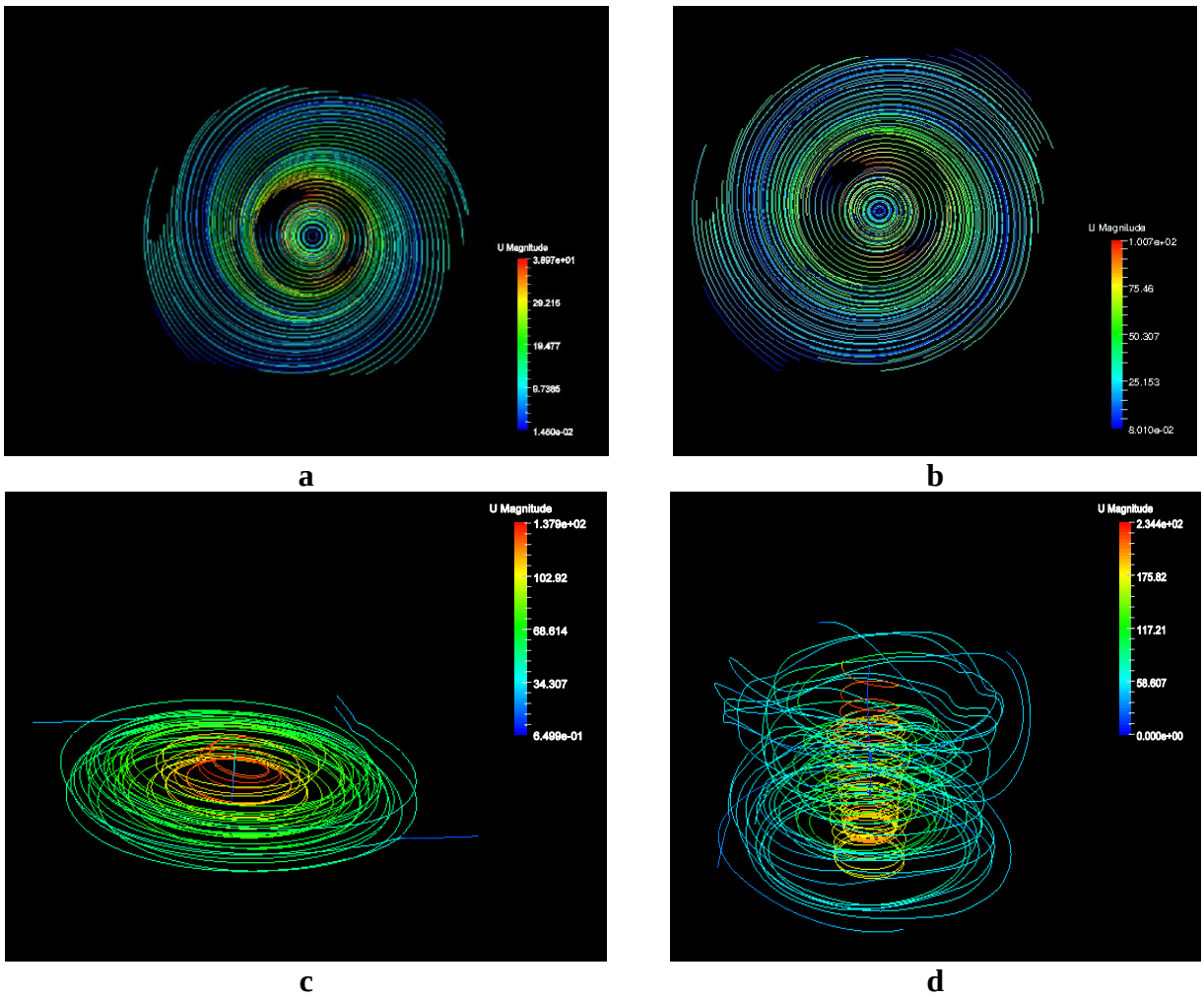

Figure 3. Relevant OpenFOAM® results for the cold-flow simulations: (a) velocity flow-field for $\dot{m}_{ox}$ = 5 g/s with combustion chamber height of 14 mm, (b) velocity flow-field for $\dot{m}_{ox}$ = 10 g/s with combustion chamber height of 14 mm, (c) vortex flow velocity for $\dot{m}_{ox}$ = 10 g/s with combustion chamber height of 14 mm, (d) vortex flow velocity for $\dot{m}_{ox}$ = 10 g/s with combustion chamber height of 54 mm.

The numerical analysis of the internal flow-field with fuel/oxidizer mixing (and without combustion modelling) is based on the Finite Volume Method (FVM) and solves for Navier-Stokes equations with RANS approach, employing the k-ε turbulence model. The code was implemented using the OpenFOAM® ReactingFoam solutor. The algorithm used for the resolution of the governing equations is based on the PISO method [18]. The boundary conditions are reported in Table 1. Fuel and oxidizer are injected inside the combustion chamber at the temperature at which they would occur in the real combustion. The injection temperature difference is the only heat transfer mechanism considered since chemical reactions and combustion are neglected. Oxidizer is injected at ambient temperature of 300 K, while the fuel enters in the chamber at the HTPB pyrolysis temperature of 800 K. The temperature gradient is set to 0 on the walls, assuming that they would not conduct heat (i.e., adiabatic walls).

DOI: 10.13009/EUCASS2017-468

Table 1: Cold flow simulation generalized boundary conditions
(T = temperature, U = velocity, k = turbulent kinetic energy, ε = turbulent dissipation).

Boundary	***T***, *K*	$\boldsymbol{p_c}$, *MPa*	***U***, *m/s*	***k***, m^2/s^2	$\boldsymbol{\varepsilon}$, m^2/s^3
Inlet	300	dP/d$\underline{n}$=0	24.5$\underline{n}$	2.25	443
Fuel	800	dP/d$\underline{n}$=0	0.001$\underline{n}$	dk/d$\underline{n}$=0	dε/d$\underline{n}$=0
Outlet	dT/d$\underline{n}$=0	1	dU/d$\underline{n}$=0/const.	dk/d$\underline{n}$=0	dε/d$\underline{n}$=0
Wall	dT/d$\underline{n}$=0	dP/d$\underline{n}$=0	U=0	dk/d$\underline{n}$=0	dε/d$\underline{n}$=0

The inlet velocity of fuel and oxidizer is fixed at inlet based on the experimental conditions evaluated in the burning tests ($\dot{m}_{ox}$ = 10 g/s). Since the cross section of the single injection channel (A) and the density of the GOX (ρ) are known, the inlet velocity is computed in each injection channel as:

$$U_{ox} = \frac{\dot{m}_{ox}}{4\rho A} \tag{1}$$

The fuel inlet velocity is imposed from the experimental regression rate typical of the hybrid rocket engine, kept constant during all the test. The no-slip condition reproduces physical walls. Hence, considering the viscosity of the gas, the fluid immediately next to the wall has null velocity. The outlet is defined by the *pressure-inlet-outlet-velocity* boundary condition. Since the modelled outlet does not represent the real operating condition, a general boundary condition was chosen to describe the outlet flow-field. It is an outlet boundary condition where the pressure is specified. The zero-gradient case is applied for outflow, while for inflow the velocity is computed from the flux in the outlet-patch normal direction. As far as the pressure is concerned, a Dirichlet boundary condition is applied to the inlets, the fuel and the walls. At the outlet, a fixed value is imposed. Considering that the velocity is almost null at the outlet, the static pressure is equal to the total one, hence it can be fixed to the camber value. This value well approximates the tested VFP operating combustion chamber pressure. Turbulence is considered to be fully developed at the injection inlets. Both k and ε gradients are set to zero at walls, outlet and fuel patches, while a fixed value is imposed at inlet. The turbulent kinetic energy is related to the turbulent intensity *I* and to the (known) mean flow velocity:

$$k = \frac{3}{2}(UI)^2 \tag{2}$$

Since a fully developed turbulence inside a complex geometry, featuring a vortex, is considered, typically the turbulence intensity is expected to be in the range 5% to 20%, as discussed in [3]. Considering a turbulent intensity of 5%, k results about 2.25 m^2/s^2. The dissipation energy is evaluated from the knowledge of the turbulent kinetic energy, based on the turbulent length scale *l*. The turbulence is taken as fully developed at the inlets, and the hydraulic diameter method is considered. The turbulence length scale is specified on the basis of the physical size of the duct as

$$l = 0.07D \tag{3}$$

Therefore, the dissipation energy is easily evaluated according to the Eq. (4),

$$\varepsilon = C_\mu \frac{k^{\frac{3}{2}}}{l} \tag{4}$$

where $C\mu$ is a model constant, having a value of 0.09 in the standard version of the k-ε model. Initial conditions are summarized in Table 2.

Table 2: Cold flow simulation initial conditions.

	T, *K*	$\boldsymbol{p_c}$, *MPa*	***U***, *m/s*	***k***, m^2/s^2	$\boldsymbol{\varepsilon}$, m^2/s^3
Initial Condition	300	1.0	0	2.25	443

Results of the simulation are shown in Figures 4-7. The Figure 4 and the Figure 5 shows the vortex flow formation in the presence of the (strong) oxidizer injection perturbing the fuel blowing from the surface. A similar behavior is shown

DOI: 10.13009/EUCASS2017-468

in the Figure 6, where focus is on the GOX flow, while Figure 7 reports the velocity magnitude in the middle x-z plane of the chamber

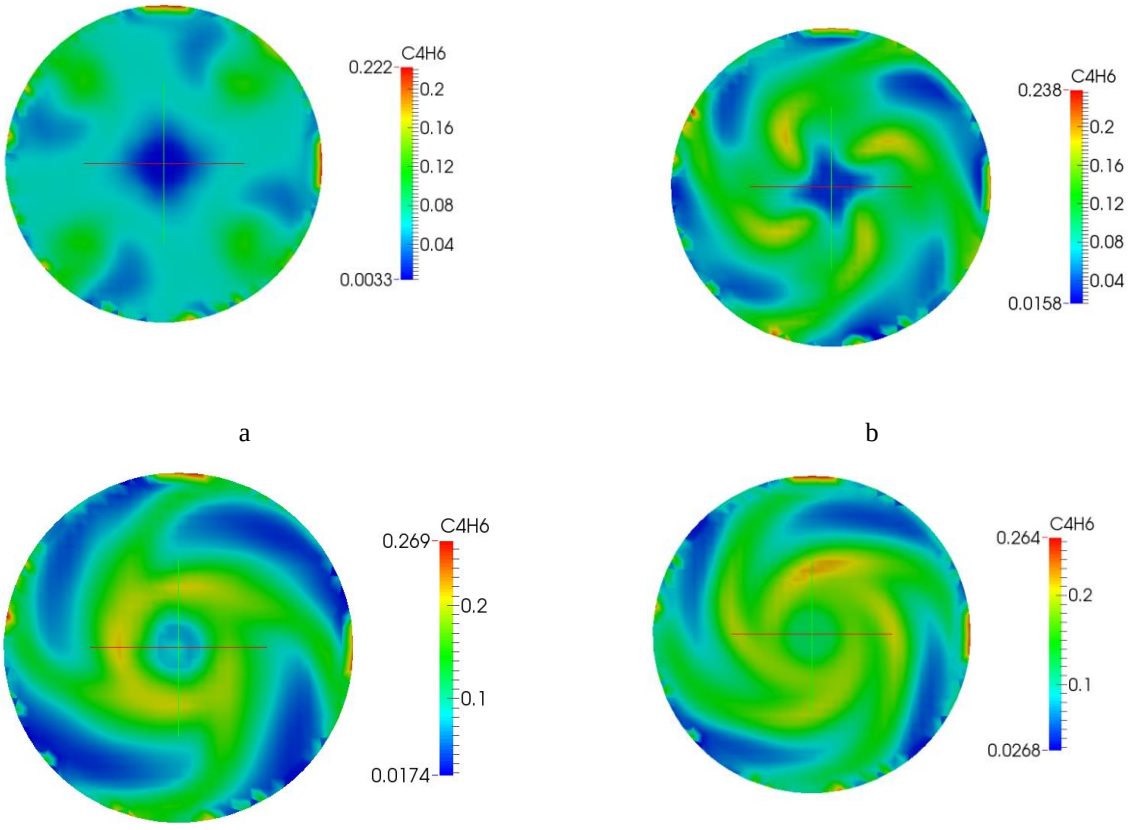

Figure 4: Evolution in time of the vaporized HTPB (i.e., C_4H_6) mass fraction at the igniter-side disk; the shown plane is 1 mm far from the fuel surface: (a) t = 0.00327 s; (b) t = 0.00729 s; (c) t = 0.00939 s; (d) t = 0.01278 s.

DOI: 10.13009/EUCASS2017-468

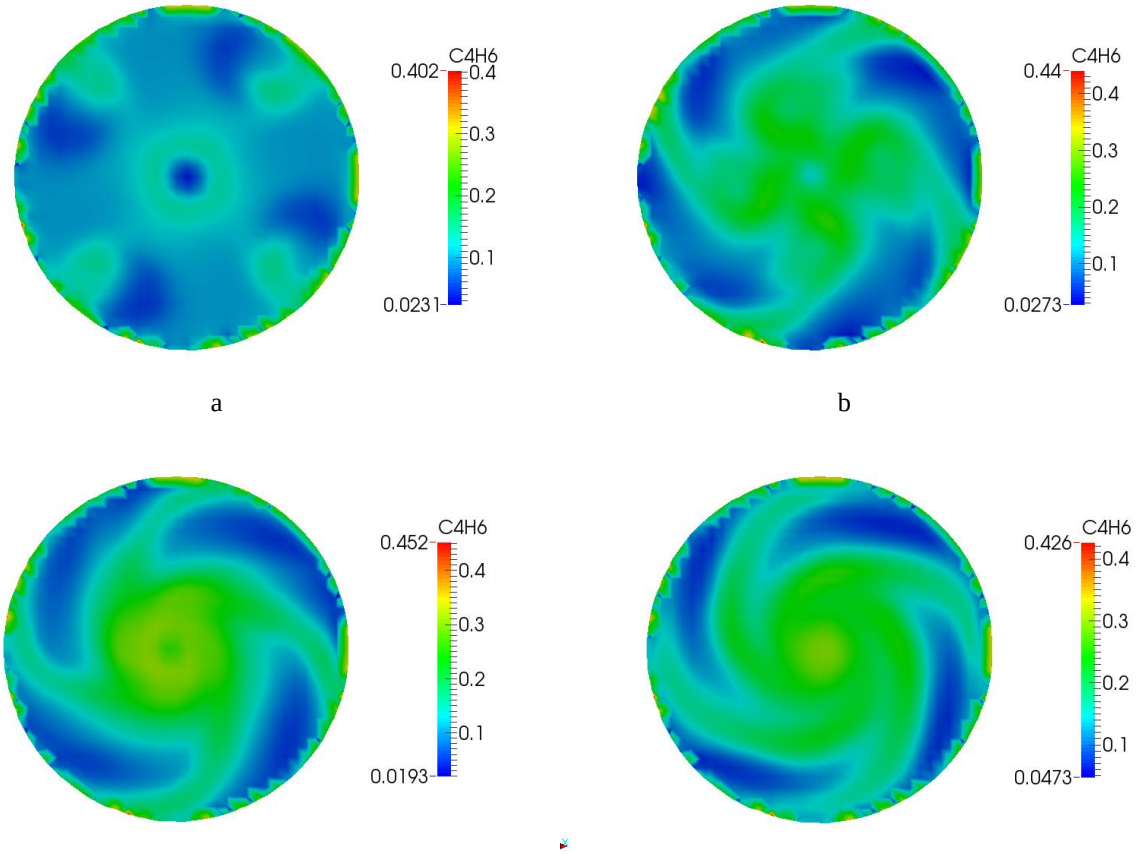

Figure 5: Evolution in time of the vaporized HTPB (i.e., C_4H_6) mass fraction at the nozzle-side disk; the shown plane is 1 mm far from the fuel surface: (a) t = 0.00327 s; (b) t = 0.00729 s; (c) t = 0.00939 s; (d) t = 0.01278 s.

DOI: 10.13009/EUCASS2017-468

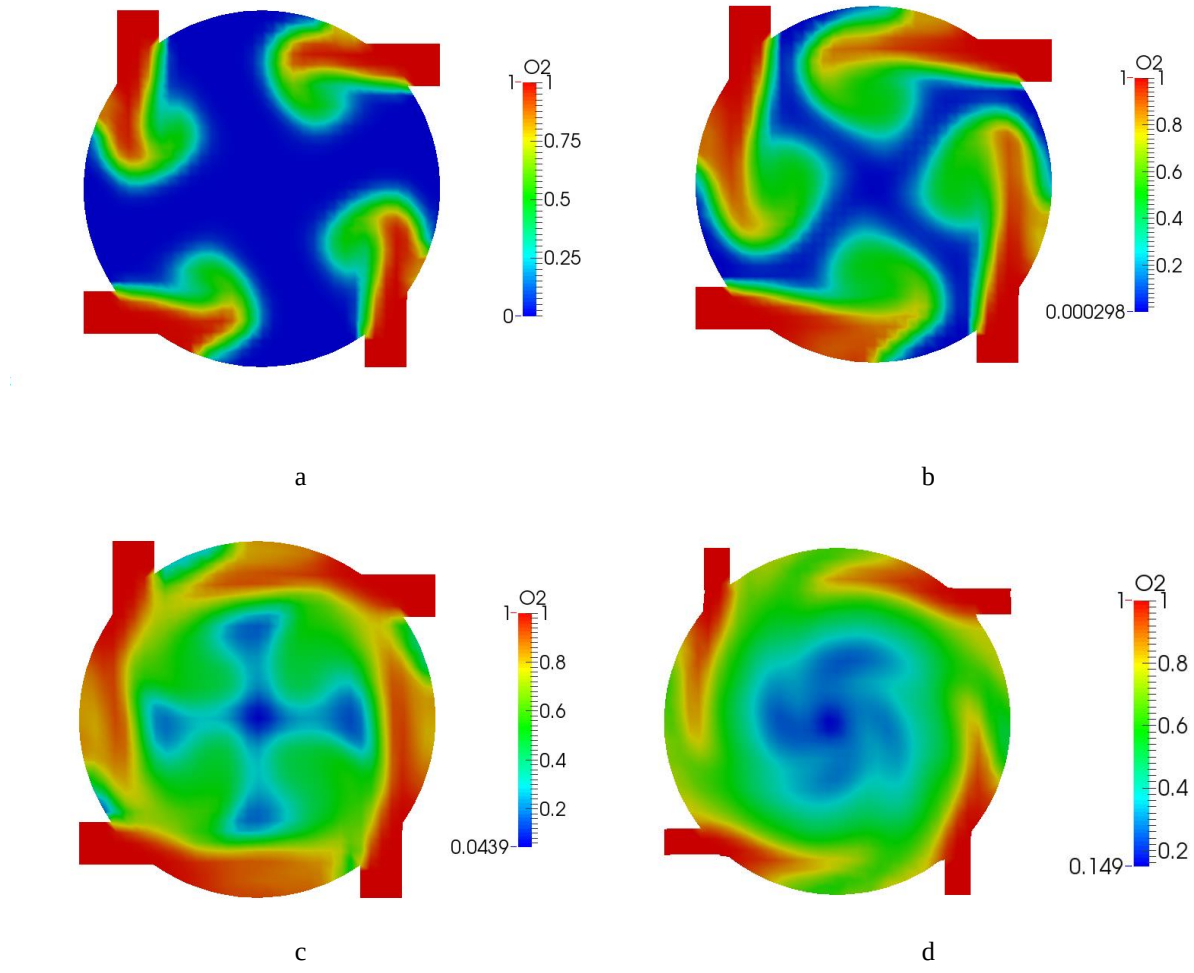

Figure 6: Oxygen concentration evolution in time in the x-z plane defined in the middle of the combustion chamber: (a) t = 0.00327 s, (b) t = 0.00537 s, (c) t = 0.00729 s, (d) t = 0.00939 s.

DOI: 10.13009/EUCASS2017-468

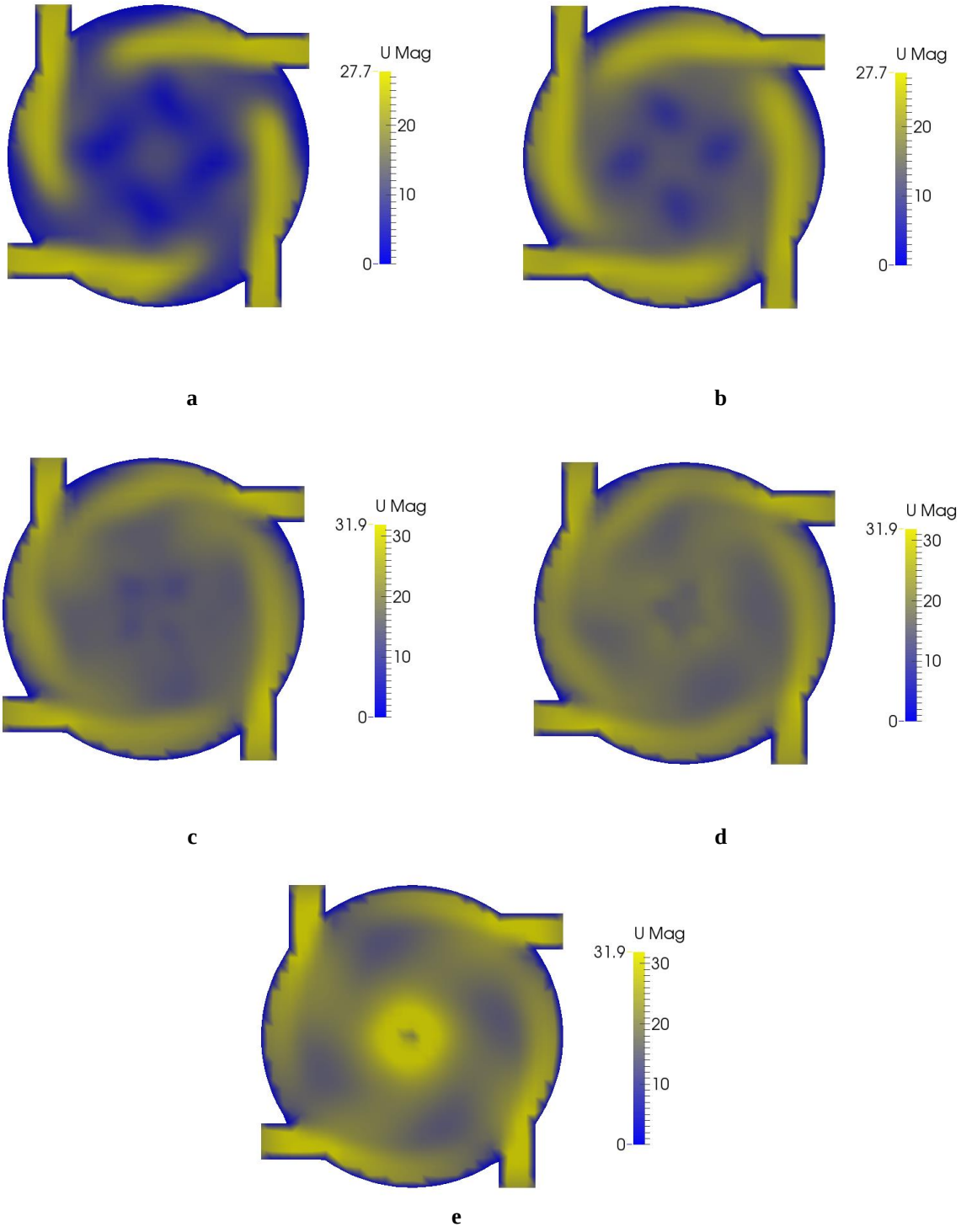

Figure 7: Vortex velocity in the combustion chamber, reference x-z plane in the middle of the chamber: (a) t = 0.00537 s, (b) t = 0.00666 s, (c) t = 0.00793 s, (d) t = 0.00862 s, (e) t = 0.0102 s.

DOI: 10.13009/EUCASS2017-468

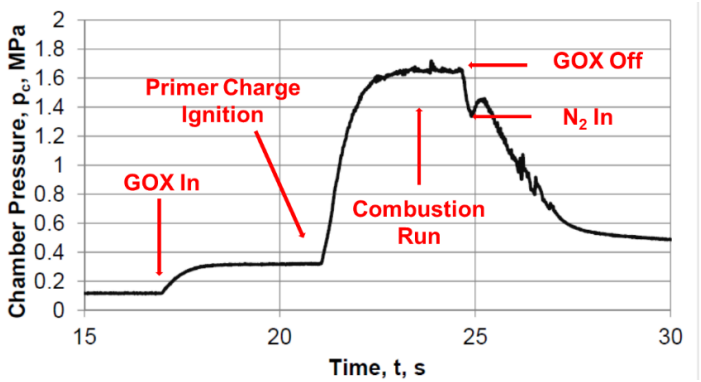

Figure 8: Typical $p_c(t)$ of a SVFP burning test.

3. Firing Tests

3.1 Quasi-steady Burning

The combustion behavior of the SVFP was tested under quasi-steady conditions, using GOX as the oxidizer, and two different fuel formulations. The first one was a paraffin-based composition where the solid wax was reinforced by a thermoplastic copolymer $SEBS_{MA}$ (styrene-ethylene-butylene-styrene grafted with maleic anhydride) [19]. The paraffin-$SEBS_{MA}$ fuel contained 40 wt% of copolymer and is therefore labelled as S40. The second tested fuel formulation is cured HTPB. The S40 was tested under oxidizer mass flow rate of 10 g/s, while the HTPB combustion runs were performed at 8 g/s. The ballistic data reduction was performed by a thickness-over-time (TOT) approach [3]. Solid fuel grains were weighted before and after the combustion run. Thus, the r_f was determined by the mass change during burning time (t_b). The latter was defined as the time interval between the reaching of the 80% of the maximum $p_c(t)$ recorded during the test, and the N_2 purge inlet (see Figure 8). The combustion efficiency (η_{c*}) of the performed combustion tests was evaluated considering the actual and the theoretical characteristic velocity (c*) values. The former was evaluated by the experimental results (average chamber pressure of the run, time-averaged overall mass flow rate) and by thermochemical calculations performed by the NASA CEA code [20-21]. The achieved experimental results are collected in the Table 3.

Table 3: SPLab VFP ballistic characterization data for S40 and HTPB fuels burning in GOX ($\dot{m}_{ox}$ of 10 and 8 g/s respectively).

Test No. (Fuel Id.)	Run No.	$\overline{p_c(t)}$, MPa	t_b, s	r_f, mm/s	η_{c*}
1 (S40)	1	1.14	2.82	0.53	0.61
	2	0.51	8.19	0.43	0.68
	3	0.54	5.46	0.38	0.71
2 (S40)	1	0.43	4.01	0.54	NAv
3 (S40)	1	0.50	1.50	1.22	NAv
	2	0.30	11.6	0.49	NAv
1 (HTPB)	1	1.65	4.77	0.50	0.93
2 (HTPB)	1	1.51	4.70	0.54	0.82
3 (HTPB)	1	1.45	3.10	0.66	0.78
	2	1.26	4.21	0.41	0.77

Tests on the propellant-grade HTPB were performed with a lower $\dot{m}_{ox}$ than the S40 runs. Despite this, the achieved r_f values resulted similar for the two formulations, while the η_{c*} shows higher values for the cured binder (see Table 3). The difference between S40 and HTPB in terms of combustion efficiency is partially due to the insurgence of marked throat erosion during the S40 tests. This inconvenience was fixed in the HTPB runs. For both S40 and HTPB, the r_f features a monotonic decrease in time. The latter result is not observed in [2]. The achieved $r_f(H_c)$ is probably due to a change in intensity of the vortex flow as

DOI: 10.13009/EUCASS2017-468

the fuel disks are consumed, and the chamber volume increases [3]. This effect is in agreement with the CFD analysis outputs (see Figure 3). While this phenomenon affects the regression rate behavior, its influence on the combustion efficiency trend appears limited. Thus, the heat transfer mechanism is strongly affected by the vortex structure. The combustion efficiency is less sensitive to the reduced vorticity since the eventual reduced mixing is compensated by an increase in the residence time of the reacting mixture in the combustion chamber. This phenomenon requires further attention. During the VFP combustion, the decreasing r_f behavior can be compensated by oxidizer mass flow rate throttling, while maintaining relatively high combustion efficiency thanks to the combustion chamber volume increase (i.e., the VFP internal volume acts as a post-combustion chamber enabling complete fuel-oxidizer reaction). On the other hand, the relatively low η_{c*} values achieved during the preliminary investigation are probably due to the limited oxidizer mass flow rates used in the test campaign. HTPB grain inspections in between the combustion runs showed regular regression surfaces, without fuel slivers accumulation in the combustion chamber or on the nozzle walls.

3.1 Forced Transient Burning

HREs undergo forced transient conditions at motor ignition/burnout, and during throttling. In the experimental campaign, the SVFP was used to investigate the effects of oxidizer mass flow rate throttling on the solid fuel behavior. Forced transient burning was investigated by a single HTPB/GOX run (see Figure 9). During the experiment, motor ignition was achieved and a first quasi-steady combustion leg was performed under $\dot{m}_{ox}$ = 8 g/s. After 3 s of combustion, the oxidizer mass flow rate was throttled down to extinction. Consequently, the SVFP $p_c(t)$ dropped from the initial value of 1.52 MPa to nearly 0.2 MPa. The oxidizer mass flow rate was then restored by a throttle-up till the the $\dot{m}_{ox}$ = 8 g/s used in the first quasi-steady leg. The actuator used for the mass flow rate interruption was based on a solenoid valve and granted a closing/opening time of 16 ms. After the throttling down transient there was a waiting time of 1.95 s. Thanks to the brief time of $\dot{m}_{ox}$interruption, the solid fuel grain was still at elevated temperature, and the hot-spots on the vaporization surface driven the motor re-ignition. A similar transient burning profile was implemented on conventional fuel grains, as discussed in [22]. The ballistic response of the solid fuel grain to the forced transient condition shows no marked overshoot/undershoot due to thermal lag effects in the condensed phase. The (faint) pressure oscillation observed after the throttle-up phase is, indeed, due to the digital flowmeter behavior. Apart from this coupling between the injection head and the combustion chamber, no significant events were recorded during the test. Considering the overall burning time of the first and of the second quasi-steady legs, the r_f evaluated in the forced transient test resulted 0.48 mm/s. This, together with the overall time-averaged chamber pressure of 1.44 MPa and the combustion time of 8.24 s confirms that the combustion behaviour of the SVFP during the forced transient was similar to an equivalent quasi-steady run.

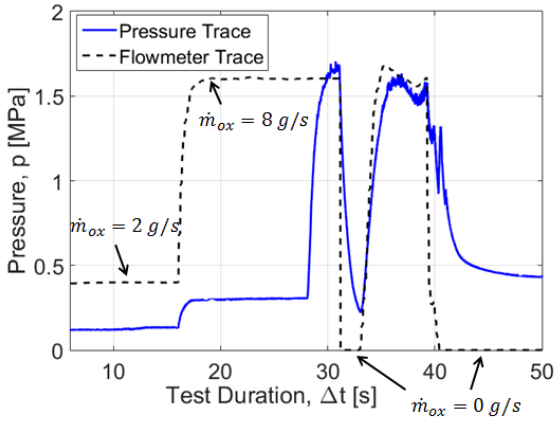

Figure 9: Forced transient combustion by oxidizer mass flow rate extinction followed by throttling up.

4. Conclusions and Future Developments

This paper discusses the ongoing SPLab activities on the investigation of a lab-scale HRE with a VFP configuration (see Figure 1). This motor promises high actual combustion efficiencies thanks to the vortex combustion, and is investigated because of its attractive features (compactness, easy implementation on different platforms) that could yield an effective use of HRE for in-space applications. The internal flow-field of the motor was investigated by CFD analyses performed by OpenFOAM®. The implemented code showed the insurgence of a vortex flow-field under the investigated condition (p_c = 1.0 MPa, $\dot{m}_{ox}$ = 10 g/s), as reported in Figures 4-7. From the experimental point of view,

DOI: 10.13009/EUCASS2017-468

combustion runs were performed on two different fuel formulations, S40 (a blended formulation of paraffin reinforced by a $SEBS_{MA}$) and HTPB. The combustion of S40 showed a peculiar behaviour with low combustion efficiencies, probably due to the characteristics of the fuel formulation. The r_f of HTPB-GOX resulted similar to the one of the S40, in spite of a reduced $\dot{m}_{ox}$ (8 g/s vs. 10 g/s). Both S40 and HTPB showed a decreasing regression rate behaviour because of the solid fuel consumption. This effect was not reported in previous VFP investigations available in the open literature [2]. During the tests, multiple ignitions were achieved and no marked combustion anisotropies were identified. The HTPB combustion showed a higher combustion efficiency than the S40. The latter resulted relatively independent from changes in the combustion chamber volume. During a forced transient burning with oxidizer mass flow rate extinction followed by a throttle-up, the SVFP showed an effective re-ignition triggered by the hot-spots on the grain surface. After the throttle-up, the $p_c(t)$ trace of the motor showed regular and stable trend, see Figure 9.

The achieved results show promising perspectives in the implementation of a hybrid propulsion-based platform enabling efficient and affordable performance and operating flexibility. Future developments of the work will focus on the expansion of the experimental matrix, and on the implementation of thrust profile measurement and actual specific impulse determination.

References

[1] Chiaverini, M.J. (2007). Review of Solid Fuel Regression Rate Behavior in Classical and Non-classical Hybrid Rocket Motors. In: *Fundamentals of Hybrid Rocket Combustion and Propulsion*, edited by M.J. Chiaverini and K.K. Kuo, Progress in Astronautics and Aeronautics, AIAA, Washington, DC, 2007, Chapter 2, pp. 37–125.

[2] Gibbon, D. M., and Haag, Lin, S., and Kwok, C. K. (2001) Investigation of an Alternative Geometry Hybrid Rocket for Small Spacecraft Orbit Transfer. *DTIC Technical Report*, AD No. 393398, 2001.

[3] Paravan, C., Glowacki, J., Carlotti, S., Maggi, F., and Galfetti, L. (2016) Vortex Combustion in a Lab-Scale Hybrid Rocket Motor. *AIAA Paper No. 2016-4562*.

[4] Marxman, G.A., and Gilbert, M. 1963. Turbulent Boundary Layer Combustion in the Hybrid Rocket. In: *9th International Symposium on Combustion*, Academic Press, Inc., New York, pp. 371-383.

[5] Marxman, G.A. 1967. Boundary Layer Combustion in Propulsion. In: *Proceedings of the 11th Symposium (International) on Combustion*, The Combustion Institute, Pittsburg, Pennsylvania, pp. 269-289.

[6] Marxman, G.A., and Wooldridge, C.E. 1968. "Research on the Combustion Mechanism of Hybrid Rockets," *Advances in Tactical Rocket Propulsion*, Edited by S.S. Penner, AGARD Conference Proceedings No. 1, pp. 421-477.

[7] Karabeyoglu, M.A., Altman, D., and Cantwell, B.J. 2002. Combustion of Liquefying Hybrid Propellants: Part 1, General Theory. *J. Prop. Power*, Vol.18, No. 3, pp. 610-620.

[8] Karabeyoglu, M.A., and Cantwell, B.J. 2002. Combustion of Liquefying Hybrid Propellants: Part 2, Stability of Liquid Films. *J. Prop. Power*, Vol.18, No. 3, pp. 621-630.

[9] Risha, G.A., Evans, B.J., Boyer, E., and Kuo, K.K. 2007. Metals, Energetic Additives and Special Binders Used in Solid Fuels for Hybrid Rockets. In: *Fundamentals of Hybrid Rocket Combustion and Propulsion*, edited by M.J. Chiaverini, and K.K. Kuo, Progress in Astronautics and Aeronautics, AIAA, Washington, DC, Chapter 10, pp. 413–456.

[10] Paravan, C. 2012. Ballistics of Innovative Solid Fuel Formulations for Hybrid Rocket Engines. Ph.D. Dissertation, Dept. of Aerospace Science and Technology, Politecnico di Milano, Milan, Italy.

[11] Yuasa, S., Shimada, O., Imamura, T., Tamura, T., and Yamamoto, K. 1999. A Technique for Improving the Performance of Hybrid Rocket Engines. *AIAA Paper No. 99-2322*.

[12] Knuth, W.A., Chiaverini, M.J., Sauer, J.A., and Gramer, D.J. 2002.Solid–fuel Regression Rate Behavior of Vortex Hybrid Rocket Engines. *J. Propul. Power*, Vol.18, No. 3, pp. 600-609.

[13] Lee, C., Na,Y., and Lee, G. 2005. The Enhancement of Regression Rate of Hybrid Rocket Fuel by Helical Grain Configuration and Swirl Flow. *AIAA Paper 2005-3906.*

[14] Wilkinson, R., Hart, K., Day, R., and Coxhill, I. 2010. Proof-of-Concept Testing of a Sustained Vortex-Flow Configuration For Hybrid Rocket Motors. *AIAA Paper No. 2010-6782.*

[15] Ohyama, S., Aso, S., Hirata, Y., Araki, K., Ohe, K., Tani, Y., and Shimada, T. 2012. A Study of Hybrid Rocket Engine with Multi-Section Swirl Injection Method. *AIAA Paper No. 2012-3905*.

[16] Rice, E. E., Gramer, D. J., St. Clair, C. P., and Chiaverini, M. J. 2003. "Mars ISRU CO/O2 Rocket Engine Development and Testing. In: *7th NASA International Microgravity Combustion Symposium*, NASA/CP—2003-212376, 2003.

[17] Majdalani, J. 2007. Vortex-injection Hybrid Rockets. In: *Fundamentals of Hybrid Rocket Combustion and Propulsion*, edited by M.J. Chiaverini, and K.K. Kuo, Progress in Astronautics and Aeronautics, AIAA, Washington, DC, Chapter 10, pp. 247-276.

DOI: 10.13009/EUCASS2017-468

[18] Barton, I. 1998. Comparison of Simple- and PISO-type Algorithms for Transient Flows. *Int. J. Numer. Methods Fluids*, Vol. 26, No. 4, 1998, pp. 459-483.
[19] Boiocchi, M., Paravan, C., Dossi, S., Maggi, F., Colombo, G., and Galfetti, L. 2015. Paraffin-based Fuels and Energetic Additives for Hybrid Rocket Propulsion. *AIAA Paper No. 2015-4042.*
[20] NASA, CEA: Chemical Equilibrium with Applications, http://www.grc.nasa.gov/WWW/CEAWeb/.
[21] Gordon, S. and McBride, B.J. 1994. Computer Program for Calculation of Complex Chemical Equilibrium Compositions and Applications, NASA Reference Publication, RP-1311.
[22] Paravan, C., Manzoni, M., Rambaldi, G., and L.T. DeLuca, "Analysis of Quasi-steady and Forced Transient Burning of Hybrid Solid Fuels in a Laboratory-scale Burner by an Optical Technique", International Journal of Energetic Materials and Chemical Propulsion, Vol. 12, Issue 5, 2013, pp. 385-420.